“Title”

Suspension pattern and rising height of sedimentary particles with low concentration in a mechanically stirred vessel

“Author name”

Yuichiro Tokura[a], Keita Miyagawa[a],Md. Azhar Uddin[a], Yoshiei Kato[a,*]

“Author address”

a: Department of Material and Energy Science, Graduate School of Environmental and Life Science, Okayama University, 1-1 Tsushima-naka, 3-chome, Kita-ku, Okayama 700-8530 Japan

“Corresponding author”

*Yoshiei Kato, E-mail address: y-kato@cc.okayama-u.ac.jp

Abstract:

In this study, the effects of impeller rotation speed, off-bottom clearance, blade angle, kinds of solid and liquid, etc. on the suspension pattern of sedimentary particles and particle-rising height in liquid were investigated with a hemispherical vessel without baffles under low particle concentration. The transition conditions of suspension pattern between regimes I and II, and regimes II and III, were observed visually, and their non-dimensional equations were expressed with a good correlation by varying the above operation factors a great deal. Here, regime I: particles stagnation on a vessel bottom II: partial suspension and III: complete suspension in liquid. The non-dimensional equation of the maximum particles-rising height was also successfully obtained. The combination of the non-dimensional equations of transition and maximum particles-rising height permitted us to determine the adequate solid/liquid mixing operation conditions without collision of particles with device parts.

Key words:

Solid/liquid mixing, Suspension, Sedimentary particle, Mechanical stirring, PIV.

1 INTRODUCTION

Mechanical stirring operations with an impeller have been used in a wide range of industries. Among them, solid/liquid mixing procedure is applied to many unit operations [1-3] such as crystallization, adsorption, solid catalytic reaction and polymerization in order to maximize solid/liquid mass transfer and reaction rates by preventing particles from depositing on a vessel bottom. [4-7] Thus, not only cloud height [8,9] above 10 mass% particle concentration but also completely suspended rotation speed were investigated by an impeller mixing with baffles. The reaction rate was moderately increased above the completely suspended rotation speed. [4, 5, 10] Thus, the empirical equations [2, 4, 11-17] and computational fluid dynamics [1, 18] were developed to estimate the completely suspended rotation speed which was one of the significant indexes.

On the other hand, crude molten metal has been purified by various methods in pyrometallurgy field. As one of the prevailing approaches to remove a small amount of nonmetallic inclusions (small-sized solid impurities) from molten light metals such as aluminum (ρ_L: 2.32x10^3 kg/m^3, T_M: 933.5 K) and magnesium (ρ_L: 1.54x10^3 kg/m^3, T_M: 923.2 K), [19] the operation procedure of addition and impeller agitation of pulverized sedimentary flux to adhere impurities has been put to practical use. [20-22] The flux amount to purify the molten metal is small due to the low impurity concentration below 1 mass%.

Thus, it is important to make clear the suspension behavior with low particle concentration for the optimal purification operation. For the metal purification procedure, the hemispherical vessel is normally used to be prevented from the flux stagnation at the bottom corner and no baffled due to the erosion by high temperature operation. In addition, unbaffled vessels have been usually used for the purification operation of molten metal in the smelting industry because baffle erosion is promoted by the metal swirl flow of high temperature.

Recently, the quest for solid/liquid mixing has become diversified to develop advanced new products. [23, 24] The collision of solid particles against device parts such as baffles and impeller or collision between solid particles sometimes reduce in products quality, [25, 26] and the impeller abrasion was also raised due to colliding with the particles. [27] For example, particle collision affected a product size distribution [25, 27] at crystallization process, abrasion of catalytic particles [25, 27] posed catalyst deterioration as well as additional process of removing the fine particles formed by the abrasion at a reactor with catalyst.

Besides, there was a need for mixing process without baffles [24] due to difficulty in cleaning baffles and cost saving in the pharmaceutical industry. Although a few studies described that the impeller mixing without baffles had smaller rotation speed and power to reach the completely suspended condition [28-30] compared with the mixing with baffles, the correlation [28, 30] of suspension behavior with the operation factors was not always found out sufficiently. There is little study on the rotation speed colliding between sedimentary particles and impeller parts. On the other hand, in the case of low concentration of solid particles with lower density than liquid, those on the liquid vortex were dispersed into the liquid phase by the collision of the deepened vortex and solid particles against an impeller when the rotation speed increased, [31] and the dispersion manner of solid particles in liquid was clarified by operation factors such as the rotation speed and off-bottom clearance.

In this study, effects of operation factors such as impeller rotation speed, off-bottom clearance, a blade angle, kinds of solid and liquid on suspension behavior of sedimentary particles were made clear by a hemispherical vessel without baffles. The hemispherical typed bottom [32] is effective for the sedimentary particles not to stagnate at the bottom of the side wall. [10] Next, the non-dimensional equations on the transitions between particles stagnation and partial suspension, and between partial and complete suspensions were formed by multi-regression analyses with the use of experimental results. The maximum particle-rising height was also indicated by the non-dimensional equation. The standard experimental condition was under the low particle concentration because it had less impact on the maximum particle-rising height as described in Chapter 3. In addition, the liquid flow pattern at the beginning of sedimentary particles suspension was visualized by a PIV system to explain the effect of impeller blade angle on the flow pattern.

2 EXPERIMENTAL

2.1 Visual observation

The suspension behavior of sedimentary particles was observed visually. The schematic diagram of experimental apparatus and angle-changeable impeller blades is shown in Figure 1. The acrylic hemispherical vessel of T [m] in inner diameter

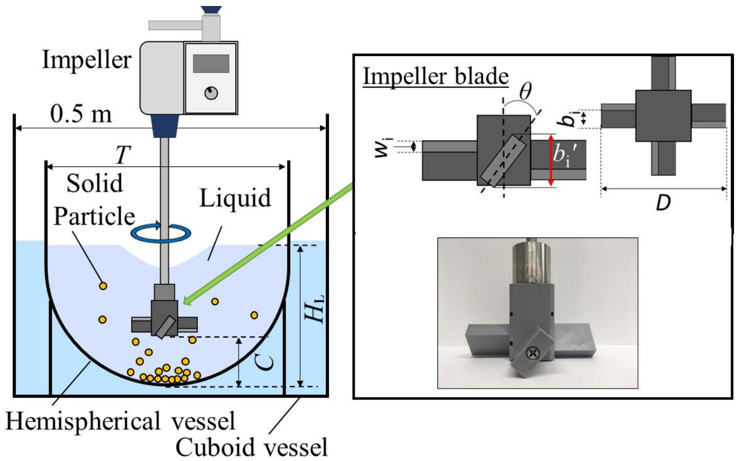

Figure 1 Schematic diagram of experimental apparatus and angle-changeable impeller blades.

without baffles was surrounded with an acrylic cuboid vessel filled with tap water to decrease optical refraction index. [33-36] Liquid was charged into the hemispherical vessel so as to become bath depth, H_L [m] = (3/5)T. Off-bottom clearance, C [m], was defined as the distance between an impeller and vessel bottoms. The shaft center of the impeller was set on the central axis of the hemispherical vessel and the up-pumping impeller was used in this study. The effect of blade angle, θ [deg], was represented by the projected thickness, b_i' [m], to liquid. [37]

$$b_i' = b_i\cos\theta + w_i\sin\theta \tag{1}$$

Here, b_i [m] and w_i [m] are the thickness and width of the blade, respectively.

Liquid used for the experiment and physical properties are shown in Table 1.

Table 1 Physical properties of liquid phase at 298.15 K.

	Liquid density, ρ_L (kg/m^3)	Liquid viscosity, μ (Pa・s)
Ion-exchanged water	0.997×10^3	0.89×10^{-3}
10 mass% glycerin-water solution	1.02×10^3	1.17×10^{-3}
20 mass% glycerin-water solution	1.05×10^3	1.55×10^{-3}

Based on ion-exchanged water (liquid density, ρ_L: 0.997x10^3 kg/m^3, liquid viscosity, μ: 0.89x10^{-3} Pas), 10 mass% glycerin-water solution (ρ_L: 1.02x10^3 kg/m^3, μ: 1.17x10^{-3} Pas) and 20 mass% glycerin-water solution (ρ_L: 1.05x10^3 kg/m^3, μ: 1.55x10^{-3} Pas) were used. On the other hand, as shown in Table 2, cationic (Na^+) exchange resin (mean diameter, d_p: 0.7×10^{-3} m, solid density, ρ_S: 1.15×10^3 kg/m^3, Organo Corporation), polystyrene ball (d_P: 1.1×10^{-3} m, ρ_S: 1.04×10^3 kg/m^3, Sekisui Plastics Co., Ltd.) and nylon ball (d_P: 3.2×10^{-3} m, ρ_S: 1.14×10^3 kg/m^3, Sato Tekko Co., Ltd.) were used for the solid particle. The kinematic viscosity

Table 2 Physical properties of solid particles.

	Solid diameter, d_S (m)	Solid density, ρ_S (kg/m^3)
Polystyrene	1.1×10^{-3}	1.04×10^3
Ion-exchange resin	0.7×10^{-3}	1.15×10^3
Nylon ball	3.2×10^{-3}	1.14×10^3

The ρ_S/ρ_L value of Na^+ exchange resin and ion-exchanged water system in this study was 1.15 as shown in Tables 1 and 2. On the other hand, the sedimentary mixed fluxes of chlorides ($MgCl_2$, KCl, NaCl, $AlCl_3$, $CaCl_2$ etc.), fluorides (NaF, KF, AlF_3 etc.), carbonates (Na_2CO_3, K_2CO_3, $CaCO_3$ etc.) are usually used to purify molten aluminum and magnesium and the densities of these compounds are between 2.0x10^3 and 3.2x10^3 kg/m^3. [20] To reach the same ρ_S/ρ_L value between this experiment and light metal purification condition, the ρ_S values of aluminum and magnesium must be 2.32x10^{3}x1.15=2.67x10^3 kg/m^3 and 1.54x10^{3}x1.15=1.77x10^3 kg/m^3, respectively. These values lay within and near the range of the flux density for aluminum and magnesium purifications, respectively. Additionally, the kinematic viscosity, μ/ρ_L, values of ion-exchanged water, molten aluminum and magnesium [38] were 8.9x10^{-7}, 5.6x10^{-7}, and

$7.1\text{x}10^{-7}$, respectively. It was found that the kinematic viscosity in this study was near the molten aluminum and magnesium. From these facts, the selection of solid-liquid system in this study seems to approximately permit to simulate the suspension behavior of flux in light molten metal.

The experimental conditions of the suspension behavior of sedimentary particles in liquid are shown in Table 3. The standard experimental conditions were shown

Table 3 Experimental conditions of suspension pattern and PIV measurements.

Variables	Suspension pattern	PIV
Vessel inner diameter, T (m)	0.2, 0.3	0.2
Bath depth (liquid height), H_L (m)	0.12, 0.18	0.12
Blade diameter, D (m)	0.088	0.088
Blade thickness, b_i (m)	0.023	0.023
Blade width, w_i (m)	0.010	0.010
Blade angle, θ (deg)	0, 40, 60, 90	0, 40, 60, 90
Rotating speed, N (s^{-1})	0 – 6.0	0.3 – 1
Off-bottom clearance, C (m)	0.024 – 0.092	0.048
Solid/liquid ratio, V_S/V_L (-)	6×10^{-4}, 0.01, 0.02	–
Continuous phase	Ion-exchanged water 10 mass% Glycerin-water solution 20 mass% Glycerin-water solution	Ion-exchanged water
Dispersed phase	Polystyrene Ion-exchange resin Nylon ball	–

underlined. The vessel diameter, T, bath depth, H_L, blade angle, θ, rotation speed, N, off-bottom clearance, C, solid/liquid volumetric ratio, V_S/V_L, and kinds of solid and liquid were varied. The experiment was carried out in the low particle concentration such as $V_S/V_L \leqq 0.02$ based on the purification process of light molten metal. Although the height of particles suspended to the entire radial direction of tank is usually measured as the cloud height in the high particle concentration situation, [9, 39] the height where low concentration of particles ($V_S/V_L \leqq 0.02$) suspend around the center axis below the impeller and impinge on the impeller was defined as the maximum rising height in this study. Each suspension behavior of sedimentary particles was determined by recording a digital video camera for 60 s to distinguish the particle suspension pattern.

The values of *Ar* number in this study were calculated between 2.13×10^2 and 5.78×10^4. The experiments were carried out in the regime where large and medium sized particles interact with turbulent eddies in the sub-range due to $Ar > 2 \times 10^{-2}$ as indicated by Grenville et al. [7]

2.2 PIV measurement

Assuming that the flow pattern with low concentration of sedimentary particles is similar to that with no-particle, the PIV experiment was carried out under the single-phase flow except for fine tracer particles. The two-dimensional PIV system (Flowtech

Research, Inc.) to measure liquid flow pattern is schematically shown in Figure 2. A neodymium laser (green) with a wavelength of 532 nm was used in this

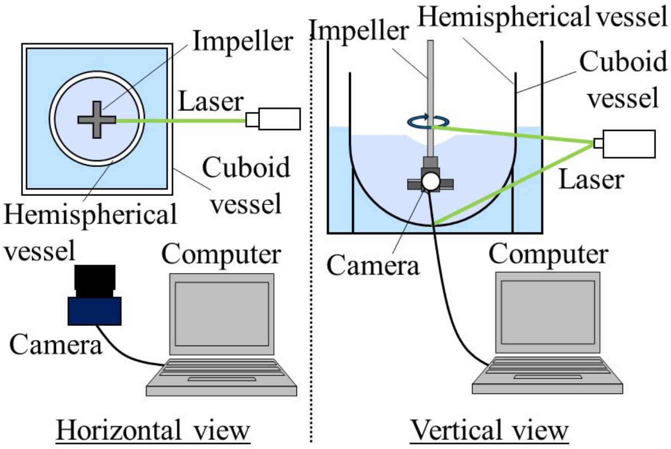

Figure 2 Schematic diagram of PIV measurement system.

system. Polystyrene particles (mean diameter: 3.05×10^{-5} m, density: 1.07×10^{3} kg/m^3, Sekisui Plastics Co., Ltd.) were put in ion-exchanged water and a black and white CCD (Charge-Coupled Device) camera was used to record the simultaneous motion of the particles in liquid. To prevent the refraction of laser beam and optical strain due to the hemispherical configuration, the cuboid vessel was filled with tap water as schematically indicated in Figure 1. The sequential 1000 frames were analyzed statistically to evaluate the liquid motion and the sampling interval was 0.005 s [36] because the reproducible flow pattern was obtained from the same test condition. The experimental conditions of PIV measurement are also shown in Table 3. The variables were blade angle and rotation speed.

3 RESULTS AND DISCUSSION

3.1 Suspension pattern of sedimentary particles in liquid

According to an increasing impeller rotation speed, sedimentary particles motion was shifted to only rotation on the vessel bottom without suspension → partially suspended in liquid → completely suspended in liquid. The particles sometimes collided with the impeller while suspending. It was visually observed from the sudden particle movement toward a direction different from fluid flow near the bottom of the impeller. As schematically shown in Figure 3, particles suspension pattern was clarified as

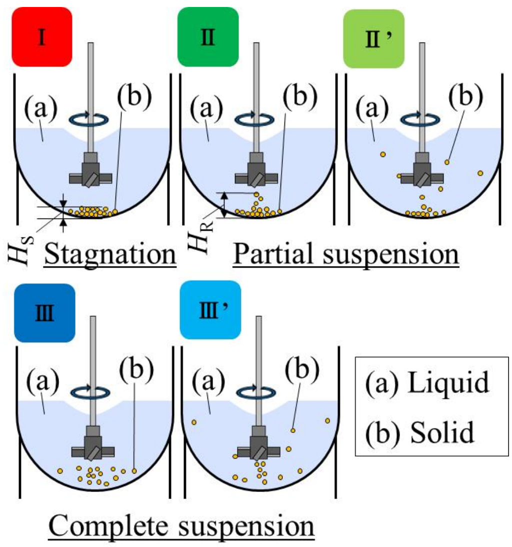

Figure 3 Schematic diagram of particles suspension patterns.

follows.

I. Regime where sedimentary particles stay at the bottom

II. Regime where particles leave the bottom partially and suspend in liquid without collision with the impeller

II'. Regime where parts of partially suspended particles collide with the impeller

III. Regime where particles leave the bottom completely and suspend in liquid without collision with the impeller

III'. Regime where parts of completely suspended particles collide with the impeller

Here, ' mark means that parts of particles collide with the impeller. In regime III or III', particles repeated to suspend in liquid within 1 to 2 seconds even if some particles deposited on the bottom based on Zwietering's definition. [4] The height of the transition between regimes II - II' (or III - III') indicates the maximum particle-rising height, H_R, of particles and becomes $C = H_R$.

In addition, an example of suspension pattern of sedimentary particles under the condition such as resin-water system, V_S/V_L=0.02, T=0.2 m, θ=40 deg and C=0.048 m is shown in Figure 4. Regime III was unobserved in this condition. The suspension pattern was switched to Regimes I→II→II"→III' by the increasing rotation speed.

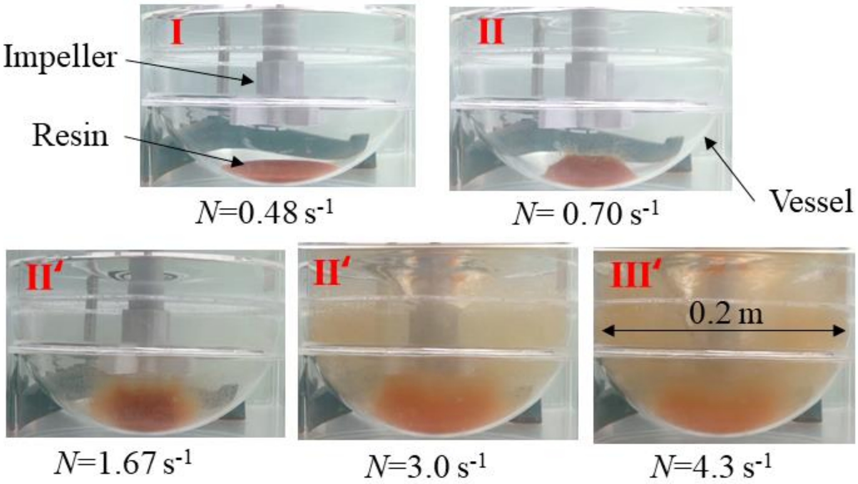

Figure 4 An example of suspension pattern of sedimentary particles

(Resin-water, V_S/V_L=0.02, T=0.2 m, θ=40 deg, C=0.048 m).

3.2 Vertical cross-sectional flow pattern

An example of cross-sectional velocity vectors obtained by the PIV measurement under the standard conditions such as T= 0.2 m, C = 0.048 m and θ = 40 deg is shown in Figure 5. The rotation speed was 1.0 s^{-1}. The condition was in regime II, although there was no sedimentary particle in the PIV system. As indicated by the arrow direction, the outward and horizontal flows generated by impeller rotation split upward and downward at the vessel wall. The upward and downward flows along the wall resulted in circulation flows, respectively. The vertical upward was seen just below the impeller blade.

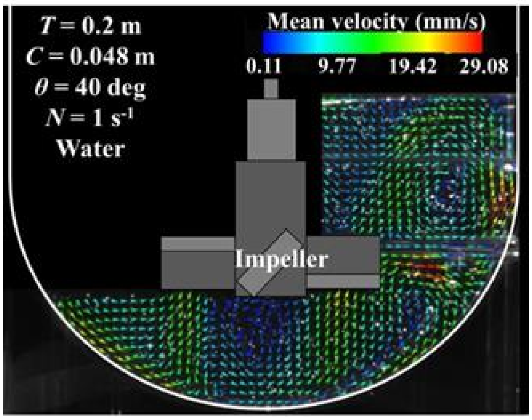

Figure 5 An example of cross-sectional velocity vectors.

3.3 Effect of operating factors on particle suspension pattern

The effect of operation factors such as off-bottom clearance, rotation speed, sedimentary particles, liquid, solid/liquid volumetric ratio, vessel diameter on the suspension pattern were investigated in this section. The relationships between the off-bottom clearance and rotation speed under the various parameters were shown together in Figure 6. The transition rotation speed of particles suspension pattern for each C in an arbitrary manner was determined when non-transition occurred at 3 % lower rotation speed. Thus, the critical rotation speed was between $0.97N$ and N. Each effect was described in detail below.

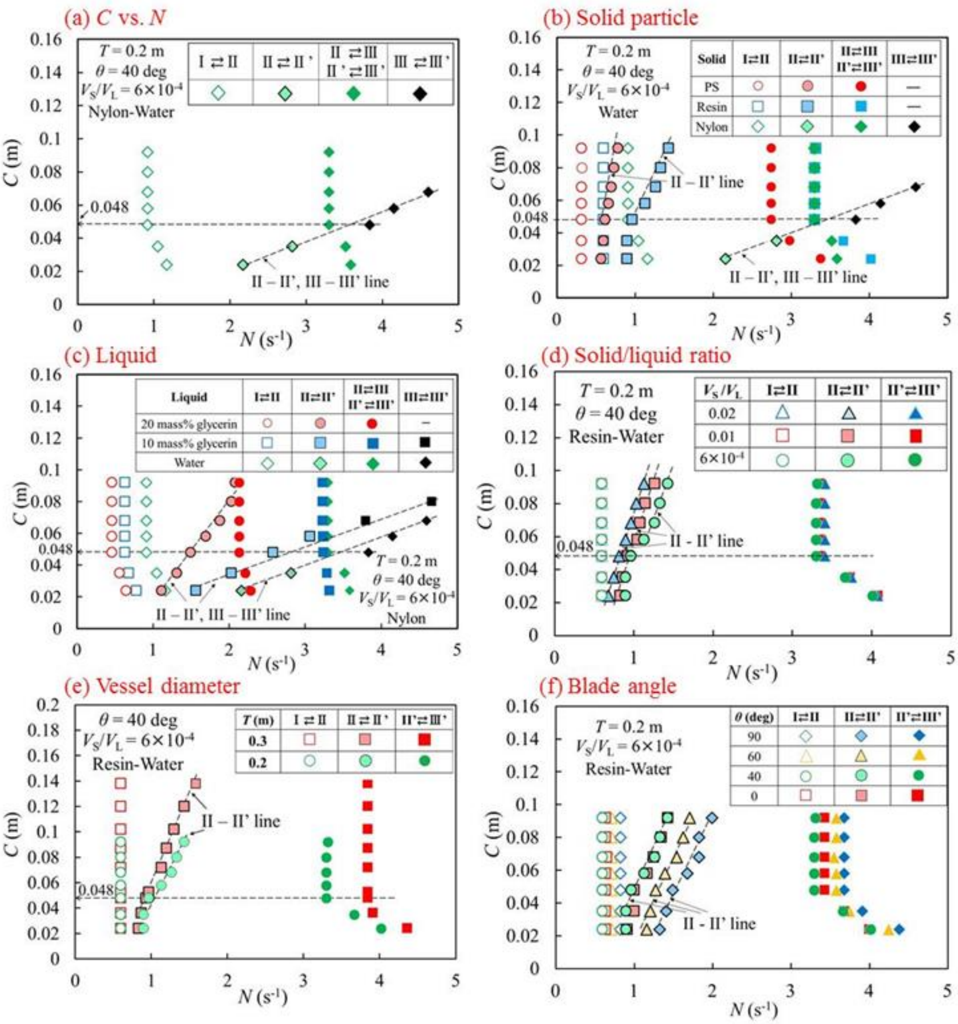

Figure 6 Effect of operating factors on transitions of particles suspension pattern.

3.3.1 Relationship between off-bottom clearance and rotation speed at transition of particles suspension pattern

The relationship between off-bottom clearance, C, and rotation speed, N, at the transition of particles suspension is shown in Figure 6 (a). The off-bottom clearance and rotation speed were varied under the standard conditions of T= 0.2 m, θ = 40 deg and V_S/V_L = 6×10^{-4} with nylon balls – ion-exchanged water system. From Figure 6 (a), both of the transition N of I - II and II–III (II' - III') were kept constant at $C \geqq 0.048$ m, whereas they increased with the decrease in C at $C < 0.048$ m. The difference of the relationship between C and N at $C = 0.048$ m is estimated to depend on the change in the flow pattern near the bottom as indicated by Montante et al. [35] The transition N of II - II' and III - III' increased with the increasing C (= H_R), which means that the maximum particle-rising height depended on the impeller rotation speed.

3.3.2 Effect of sedimentary particles and liquid on their suspension pattern

The effect of solid particles on the transition of particles suspension pattern is shown in Figure 6 (b). Three kinds of solid particles were used. $T = 0.2$ m, $\theta = 40$ deg, $V_S/V_L = 6\times10^{-4}$ and ion-exchanged water were the standard conditions. The transition between C and N of each kind of particles indicated had almost the same tendency as Figure 6 (a). The transition N of I - II and II - III (II' - III') against C was in the following descending order: Nylon ball > Ion exchange resin > Polystyrene (PS), except the transition of II–III (II' - III') for resin and nylon, that is, 0.92 s^{-1} (Nylon) > 0.60 s^{-1} (resin) > 0.32 s^{-1} (PS) for I – II, and 2.75 s^{-1} (Nylon) > 3.3 s^{-1} (resin and PS) for II - III (II' - III'). It is due to the higher density and diameter of particles which make it more difficult to suspend in liquid. [40] Being different from nylon ball, the I - II transition N for polystyrene and resin was kept constant at $C < 0.048$ m because of suspension easiness. However, the II - III (II’ - III’) tendency of N vs C was the same between three solid particles. Moreover, the transition N of II - II’ and III - III’ increased with the increasing C (= H_R).

The effect of physical properties of liquid phase such as density and viscosity on the transition of nylon particles suspension pattern is shown in Figure 6 (c). T = 0.2 m, θ = 40 deg and $V_S/V_L = 6\times10^{-4}$ were the standard conditions. The transition N of I - II and II - III (II’ - III’) against C was in the following descending order: water > 10 mass% glycerin-water solution > 20 mass% glycerin-water solution, although the relationship between transition N and C had the same tendency as Figures 6 (a) and (b). That was due to the larger liquid viscosity, which was easy to lift up and difficult to sink down the solid particles. On the other hand, the transition N of regime II - II’ and III - III’ increased with the increasing C (= H_R).

3.3.3 Effect of solid/liquid volumetric ratio on suspension pattern of sedimentary particles

The effect of solid/liquid volumetric ratio, V_S/V_L, on the resin suspension pattern is shown in Figure 6 (d). The ion-exchange resin was used as the sedimentary particles. T = 0.2 m and θ = 40 deg were the standard conditions. From Figure 6 (d), neither C nor V_S/V_L was almost affected by the transition N of I – II and II’ – III’. The smaller V_S/V_L

made the transition N of II – II' slightly larger against the same C, although the difference was smaller than those of other figures in Figure 6. Thus, the suspension behavior with low sedimentary particle concentration was permitted to estimate the suspension with the other concentration. There was no III regime in this condition. That is because some particles begin to collide with the impeller before the complete suspension.

3.3.4 Effect of vessel diameter on suspension pattern of sedimentary particles

The effect of vessel diameter on the transition of resin particles suspension pattern is shown in Figure 6 (e) when the ion-exchange resin was used as the sedimentary particles. $\theta = 40$ deg and $V_S/V_L = 6\times10^{-4}$ were the standard conditions. The transition N of I – II at $T = 0.2$ and 0.3 m became equal to each other and constant for varying C. On the other hand, the transition N of II' – III' was kept constant at $C \geqq 0.048$ m and larger at $C < 0.048$ m as seen in Figures 6 (a) – (d), and that of $T = 0.3$ m had the larger N than $T = 0.2$ m. As the energy supplied rate per volume of $T = 0.2$ m was larger than that of T =0.3 m at the more strong rotation speed such as $N > 3$ s^{-1}, all particles suspended in the liquid phase even if the rotation speed of $T = 0.2$ m was smaller than that of $T = 0.3$ m. The maximum particle-rising height, H_R, of $T = 0.2$ m obtained from the transition C of II - II' was slightly smaller than that of $T = 0.3$ m at the same rotation speed. That results from the smaller geometric configuration of T = 0.2 m. C normalized by T indicated the same values between T = 0.2 and 0.3 m, although it was not shown by the figure.

3.3.5 Effect of blade angle on particles suspension and liquid flow patterns

The effect of blade angle on the transition of resin particles suspension pattern is shown in Figure 6 (f) when the ion-exchange resin as the sedimentary particles and water as liquid phase were used. T = 0.2 m and $V_S/V_L = 6\times10^{-4}$ were the standard conditions. Both of the transition N of I - II and II' - III' for a given C were in the following ascending order: θ = 40 < 0 < 60 < 90 deg. Liquid circulation flow caused by the impeller rotation is promoted by the larger blade-projected thickness promotes when the rotation speed is equal. The blade-projected thickness calculated by Equation (1) was in the following decreasing order: θ = 40 (b_i'=0.024 m), > 0 (b_i'=0.023 m) > 60 (b_i'=0.020 m) > 90 deg (b_i'=0.010 m). Thus, the blade-projected thickness decreased the transition N at the same C. The maximum particle-rising height, H_R obtained by the transition C of II - II' at the same N was also in the following descending order: θ = 40 > 0 > 60 > 90 deg.

When the uplifting force of particles on the bottom surpasses the difference of downward force between gravity and buoyancy, they start suspending in liquid [5] and the transition of I - II occurs. The upward force associated with liquid flow near the bottom is supposed to affect the particles suspension. Taking notice of the upward vertical velocity, the PIV measurements at different blade angle were carried out under the standard conditions of $T = 0.2$ m, $C = 0.048$ m and $V_S/V_L = 6\times10^{-4}$. The impeller rotation speed at the transition of I－II was used for each blade angle as seen in Figure 6 (f).

Figure 7 shows the distribution of the upward vertical mean velocity under the impeller by a PIV measurement. Each figure was drawn by vertical components of velocity vector as typically shown in Figure 5. The rotation speed of each impeller blade in Figure 7 was at the transition of I – II. For four kinds of blade angles, there was an

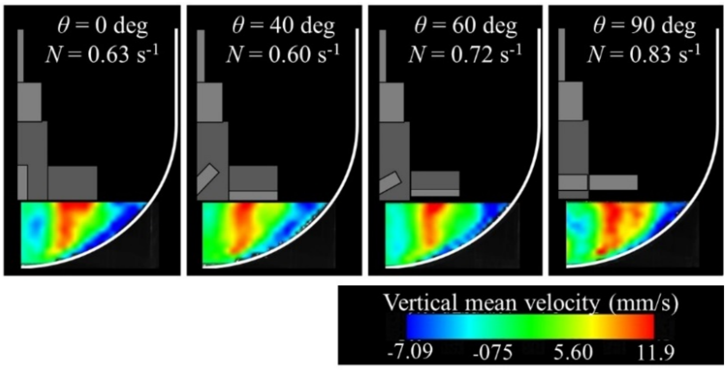

Figure 7 Distribution of upward vertical mean velocity for different blade angle.

upward flow just below the blade as indicated in red color, whereas a downward flow in blue color along the curved wall. Each upward vertical velocity was almost equal at the transition N of I - II. This upward flow seems to result in the force of particles lifting-up. On the other hand, each power number, N_P, of the condition in Figure 7 was calculated by Nagata's formula [41] applicable to the homogeneous stirring without baffles as follows:

0.915 (θ = 40 deg, b_i' = 0.024 m, N = 0.6 s^{-1}), 0.877 (θ = 0 deg, b_i' = 0.023 m, N = 0.63 s^{-1}), 0.779 (θ = 60 deg, b_i' = 0.020 m, N = 0.72 s^{-1}) and 0.504 (θ = 90 deg, b_i' = 0.010 m, N = 0.83 s^{-1}), that is, N_p decreased with the decreasing b_i' and increasing N.

In this study, the suspension pattern of sedimentary particles was investigated under the up-pumping operation where upward flow was formed just below the blade as seen in Figure 7. The necessary comparison between the up- and down-pumping conditions may be made in the next phase.

3.4 Non-dimensional equations of particles suspension pattern and maximum particle-rising height in liquid

From Section 3.3, the transition N did not affect C at $C \geqq 0.048$ m where two circulation flow existed below and above C. In this section, non-dimensional equations of the transition of I-II and II - III (II' - III') at $C \geqq 0.048$ m were developed by a multiple regression analysis with dimensionless variables. The maximum particle rising height, H_R in liquid calculated by the transition C of II - II' and III - III' was also offered by another multiple regression analysis.

The non-dimensional equation of the transition of I - II, that is, the initiation of sedimentary particle suspension in liquid was obtained as follows:

$$Fr = 10^{-4.75} Re^{0.895} \{(\rho_\mathrm{S} - \rho_\mathrm{L})/\rho_\mathrm{L}\}^{0.651} (b_\mathrm{i}'/D)^{-0.434} (d_\mathrm{p}/D)^{0.367} \tag{2}$$

Here, as the transition of I - II is considered to be affected by 8 variables such as D, N, g, ρ_L, μ_L, ρ_S, b_i' and d_P, and they have 3 basic units like length, time and mass, 5 (=8-3) sorts of dimensionless variables are necessary according to Buckingham's Π theorem. Thus, 5 dimensionless variables in Equation (2) were used for the non-dimensional equation. Equation (2) can be arranged by the Zwietering equation form [4] as follows:

$$N_\mathrm{JS}^{*} = 3.97\mathrm{x}10^{-4}\, \nu^{-0.810} \{(\rho_\mathrm{S} - \rho_\mathrm{L})/\rho_\mathrm{L}\}^{0.589}\, b_\mathrm{i}'^{-0.393}\, d_\mathrm{p}^{0.332}\, D^{-0.776} \tag{2'}$$

Here, the impeller rotation speed at the transition of regime I and II, N_JS^{*}, had a positive correlation with the particle diameter, d_P, and a negative one with the impeller diameter, D, as well as Zwietering equation [4].

The relationship between the measured and calculated Fr is shown in Figure 8. A

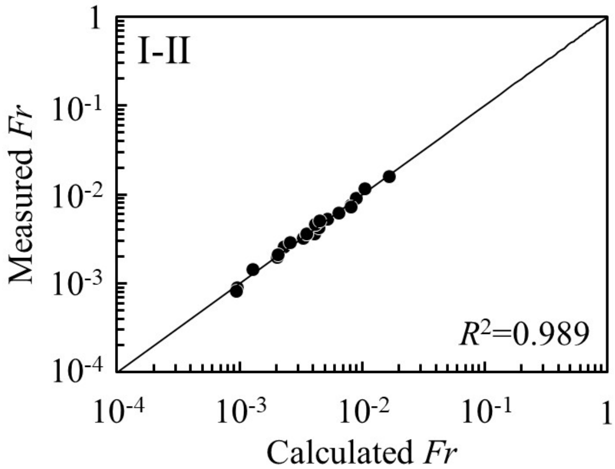

Figure 8 Comparison between measured and calculated *Fr* at the transition of I - II.

good correlation was achieved (R^2 = 0.989). As *Fr* and *Re* in Equation (2) represent inertial force/gravitational force and inertial force/viscous force, respectively, $Fr/Re^{0.895}$ indicates (inertial force)$^{0.105}$. Thus, the inertial force at the transition of I – II had a positive correlation with $(\rho_\mathrm{S} - \rho_\mathrm{L})$ and d_P, and a negative correlation with b_i'. It means that the larger $(\rho_\mathrm{S} - \rho_\mathrm{L})$ and d_P values needed the extra inertia to suspend a particle, whereas the larger b_i' agitates solid/liquid effectively and reduced the rotation speed.

Next, the non-dimensional equation of the transition of II - III and II' - III' was given by Equation (3).

$$Fr = 10^{-4.45} Re^{0.806} \{(\rho_\mathrm{S} - \rho_\mathrm{L})/\rho_\mathrm{L}\}^{0.227} (b_\mathrm{i}'/D)^{-0.110} \qquad (3)$$

Here, 4 kinds of dimensionless variables in Equation (3) were selected. Figure 9 (a)

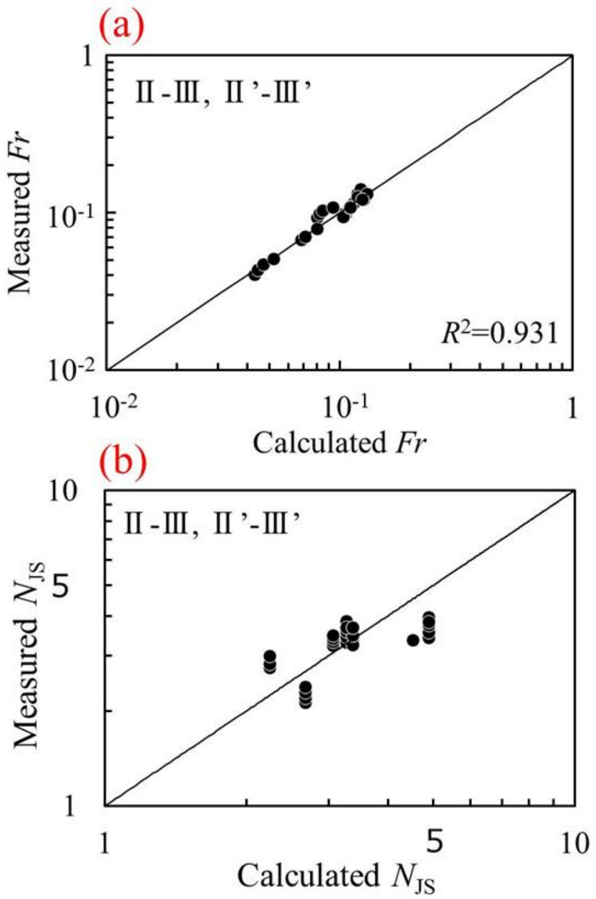

Figure 9 Comparison between measured and calculated *Fr* number (a) and N_{JS} by Tamburini et al. [30] at the transition of II – III and II' – III'.

shows the comparison between measured and calculated *Fr* at the transition of II - III and II' - III'. They had a good correlation of R^2=0.931. On the other hand, another multiple regression analysis including particle diameter was obtained as Equation (3).

$$Fr = 10^{-4.48} Re^{0.812} \{(\rho_S - \rho_L)/\rho_L\}^{0.217} (b_i'/D)^{-0.093} (d_p/D)^{-0.010} \quad (3')$$

Here, R^2 became 0.969. However, as the exponent of (d_p/D) term came to -0.01, the effect of particle diameter on the transition of II - III and II' - III' was negligibly small as well as Tamburini et al. [30] That seems to be because the fluid inertial force is significantly larger than the fluid resistance working on particles unlike in the case of the transition of I - II. Thus, Equation (3) is better than Equation (3') as the non-dimensional equation of the transition of II - III and II' - III'. $Fr/Re^{0.806}$ from Equation (3) indicates (inertial force)$^{0.194}$. As well as Equation (2), larger $(\rho_S - \rho_L)$ increased the inertia and larger b_i' decreased the rotation speed.

On the other hand, the equation of rotation speed to predict the complete suspension pattern of particles was given by Tamburini et al. (2014) as follows:

$$N_{JS} = K\, d_P^{\,0.033} \{g(\rho_S - \rho_L)/\rho_L\}^{0.309} B^{0.115} \nu^{-0.143} \qquad (4)$$

By substituting V_S/V_L into B which is defined as the particles concentration in liquid (m^{-3}), the scale parameter, K, was deformed as Equation (4')

$$K = N_{JS} / [d_P^{\,0.033} \{g(\rho_S - \rho_L)/\rho_L\}^{0.309} V_S/V_L^{\,0.115} \nu^{-0.143}] \qquad (4')$$

The mean K value was calculated as 1.17 by the experimental values in this study. The relationship between the experimental and calculated N_{JS} values is shown in Figure 9 (b). The change in the experimental values became smaller than the calculated ones compared with Figure 9 (a).

The non-dimensional equation of the maximum particle-rising height (= off-bottom clearance at the transition of II - II’ and III - III’), which may be used in a limited way to obtain the avoiding condition of the collision between particles and an impeller, was indicated by Equation (5).

$$Fr = 10^{-4.29} Re^{1.11} \{(\rho_\mathrm{S} - \rho_\mathrm{L})/\rho_\mathrm{L}\}^{0.529} \{(C - H_\mathrm{S})/T\}^{0.329} (b_\mathrm{i}'/D)^{-0.437} (d_\mathrm{p}/D)^{0.809} \quad (5)$$

Here, there were 10 variables such as D, N, g, ρ_L, μ_L, ρ_S, b_i', d_p, T and (C-H_s) including 3 basic units (length, time and mass). Although Buckingham’s Π theorem demands 7 (=10-3) dimensionless variables, a good correlation (R^2=0.989) was achieved by even 6 dimensionless variables in Equation (5) as shown in Figure 10.

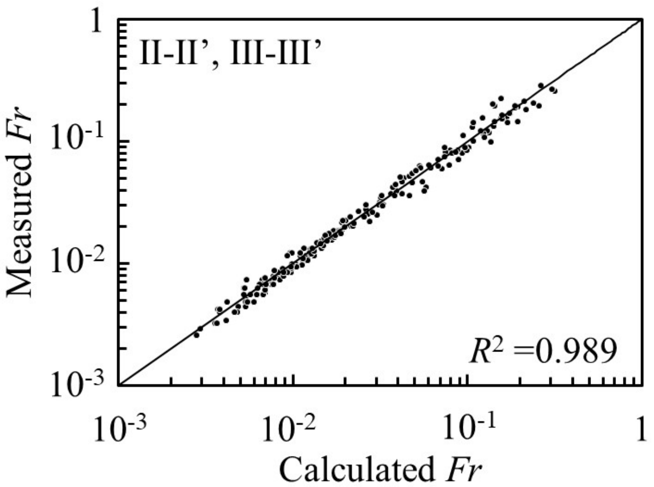

Here,

Figure 10 Comparison between measured and calculated Fr at the transition of II - II’ and III - III’ (maximum rising height of particles).

the effect of V_S/V_L on the maximum particle-rising height was included by H_s term in Equation (5). From Equation (5), the $(C-H_S)$ term relevant to the maximum rising height had a negative correlation with $(\rho_S - \rho_L)$ and d_P due to the fluid resistance acting on particles, whereas it maintained mutually positive relationship with b_i' and $Fr/\mathrm{Re}^{1.11} \propto N^{0.89}$ because of the increasing power.

Thus, the adequate solid/liquid mixing operation factors to avoid particles collision with device parts such as an impeller, baffles, etc. will be determined by combining the transition of regime I - II (Equation (2)) or II - III (Equation (3)) with the maximum particle rising height (Equation (5)).

Non-dimensional equations of Equations (2), (3) and (5) were given by some dimensionless number such as *Re*, *Fr*, and not by the power number, N_p, because N_p is seemed to be essentially a function of *Re* and *Fr*, and was not measured in this study. However, the relationship between *Re*, *Fr* and N_p will be evaluated in this suspension condition of sedimentary particles by obtaining N_p from the measurement of the power required for stirring, *P*, in the future.

There are two scale-up criteria of stirring apparatus in terms of dynamic similarity: constant power per unit volume and tip velocity. [42] The constant power per unit volume leads to $N \propto b_i'^{-2/3}$ and constant tip velocity to $N \propto b_i'^{-1}$. On the other hand, Equations

(2), (3) and (5) became $N \propto b_i'^{-0.393}$, $N \propto b_i'^{-0.092}$ and $N \propto b_i'^{-0.491}$, respectively. The exponent of b_i' (-0.491) for the particle rising height in Equation (5) was a 26.4 % difference and roughly close to that of b_i' (-2/3) for the criterion of the power per unit volume, compared with the transition of the regime I-II and II-III which did not fit into either criteria for power per unit volume or tip velocity. The analysis based on the individual particle motion in fluid will be necessary to obtain the appropriate scale-up rule for these transitions in the future.

4 CONCLUSIONS

The effects of off-bottom clearance, impeller rotation speed, blade angle, a few kinds of solid particles and liquid, etc. on the suspension pattern of sedimentary particles in liquid were investigated by a hemispherical vessel without baffles.

- The transition of rotation speed between the regimes I (particles stagnation) - II (partial suspension) as well as II (partial suspension) - III (complete suspension) was kept constant above a given off-bottom clearance and increased below it.
- The vertical upward velocity near a vessel bottom became equal at the transition of the regime I - II.

- The non-dimensional equations of transitions of regimes I - II and II - III with a good correlation were obtained by 4 or 5 kinds of dimensionless variables.
- The maximum particle-rising height was successfully given by the non-dimensional equation with 6 kinds of dimensionless variables.

Nomenclature

Ar: Archimedes number defined by $d_p^3(\rho_S - \rho_L)\,\rho_L g/\mu^2$

b_i: Impeller thickness defined by Figure 1 [m]

b_i': Projected thickness defined by Equation (1) [m]

B: Particles concentration in liquid defined by Tamburtini et al. [30]

C: Off-bottom clearance [m]

d_p: Particle diameter [m]

D: Impeller diameter [m]

Fr: Froude number defined as DN^2/g

g: Gravity acceleration [m/s^2]

H_L: Bath depth [m]

H_R: Maximum particle-rising height [m]

H_S: Thickness of sedimentary particles layer [m]

K: Scale factor defined by Tamburtini et al. [30]

N: Impeller rotation speed [s^{-1}]

N_{JS}: Impeller rotation speed at the transition of regime II and III [s^{-1}]

N_{JS}^*: Impeller rotation speed at the transition of regime I and II [s^{-1}]

N_P: power number defined as $P/(\rho_L N^3 D^5)$

P: Power required for stirring [W]

Re: Reynolds number defined by $\rho_L N D^2/\mu_L$

T: Vessel inner diameter [m]

T_M: Melting point [K]

V_S: Solid particles volume [m^3]

V_L: Liquid volume [m^3]

w_i: Impeller width defined by Figure 1 [m]

ρ_L: Liquid density [kg/m^3]

ρ_S: Solid density [kg/m^3]

θ: Blade angle [deg]

μ : Liquid viscosity [Pa・s]

v: Kinematic viscosity [m^2/s] defined by μ/ρ_L

References

(1) S. Hosseini, D. Patel, F. Ein-Mozaffari, M. Mehrvar, *Ind. Eng. Chem. Res.* **2010**, 49, 4426.

(2) S. Aravinth, P. G. Rao, T. Murugesan, *Bioproc. Eng.* **1996**, 14, 97.

(3) P. M. Armenante,E. U. Nagamine, J. Susanto, *Can. J. Chem. Eng.* **1998**, 76, 413.

(4) T. N. Zwietering, *Chem. Eng. Sci.* **1958**, 8, 244.

(5) Z. Zamzam, S. Yoshikawa, S. Ookawara, Y. Kato, *J. Chem. Eng. Japan.* **2016**, 49, 737.

(6) E. Y. Bong, N. Eshtiaghi, J. Wu, R. Parthasarathy, *Chem. Eng. Res. Des.* **2015**, 100, 148.

(7) R. Grenville, A. T. C. Mak, D. A. R. Brown, *Chem. Eng. Res. Des.* **2015**, 100, 282

(8) V. Madhavi, M.V. Sardeshpande, A. R. Sagi, V. A. Juvekar, V. V. Ranade, *Ind. Eng. Chem. Res.* **2009**, 48, 9713.

(9) K. J. Bittorf, S. M. Kresta, *Trans. IChemE.* **2003**, 81, Pat A, 568.

(10) S. Nagata, T. Yokoyama, S. Nanjyo, *Kagaku kogaku* **1953**, 17, 98.

(11) S. Nagata, T. Yokoyama, H. Naka, *Kagaku kogaku* **1953**, 17, 144.

(12) A. W. Nienow, *Chem. Eng. Sci.* **1968**, 23, 1453.

(13) S. Narayanan, V. K. Bhatia, D. K. Guha, M. N. Rao, *Chem. Eng. Sci.* **1969**, 24, 223.

(14) K. Wichterle, *Chem. Eng. Sci.* **1988**, 43, 467.

(15) G. Baldi, R. Conti, E. Alaria, *Chem. Eng. Sci.* **1978**, 33, 21.

(16) R. Conti, S. Sicardi, V. Specchia, *The Chemical Engineering Journal* **1981**, 22, 247.

(17) P. M. Armenante, E. U. Nagaminea, *Chem. Eng. Sci.* **1998**, 53, 1757.

(18) Y. Shoji, N. Yoshio, M. Tanaka, K. Otawara, *Kagaku kogaku ronbunsyu* **2018**, 44, 39.

(19) The Japan Institute of Metals and Materials, *Handbook of Metallurgy*, Rev. 6th ed. Maruzen, Tokyo **2000**, P. 565

(20) S. Nishina, *Keikinzoku* **1991**, 41, 373

(21) G-H Wu, W. Wang, M. Sun, Q-D. Wang, W-J. Ding, *Trans. Nonferrous Metals Society China*, **2010**, 20, 1177

(22) J. Mei, W-C. Liu, G-H.Wu, Y. Zhang, Y-T. Zhang, Y-K. Hong, R-X. Zhang, L. Xiao, W-J. Ding, *Trans. Nonferrous Metals Society China*, **2015**, 25, 1811

(23) N. Kamei, Y. Kato, Y. Tada, T. Murai, J. Ando, *Kagaku kogaku ronbunsyu* **2008**, 34, 551.

(24) K. J. Myers, J. P. Herr, E. E. Janz, *Can. J. Chem. Eng.* **2011**, 89, 940.

(25) J. J. Derksen, *AIChE J.* **2003**, 49, 2700.

(26) X. Shan, G. Yu, C. Yang, Z. S. Mao, W. Zhang, *Ind. Eng. Chem. Res.* **2008**, 47, 2926.

(27) M. Isaji, S. Ookawara, K. Ogawa, *Kagaku kogaku tonbunsyu* **2006**, 32, 315.

(28) A. Tamburini, A. Cipollina, G. Micale, F. Scargiali, A. Brucato, *Ind. Eng. Chem. Res.* **2016**, 55, 7535.

(29) B. M. Cohen, B. Inankur, K. T. Lauser, J. Lott, W. Chen, Org. *Process Res. Dev.* **2018**, 22, 1481.

(30) A. Tamburini, A. Brucato, A. Busciglio, A. Cipollina, F. Grisafi, G. Micale, F. Scargiali, G. Vella, *Ind. Eng. Chem. Res.* **2014**, 53, 9587.

(31) R. Shiba, Md. A. Uddin, Y. Kato, *Tetsu-to-Hagane* **2016**, 102, 196.

(32) Y. Kato, K. Shiobara, H. Furukawa, Y. Tada, Y. Nagatsu, S. T. Koh, Y. S. Lee, *Kagaku kogaku ronbunsyu* **2011**, 37, 305.

(33) Y. Takahashi, M. Iguchi, *Tetsu-to-Hagane* **2008**, 94, 461.

(34) R. Tanaka, Md. A. Uddin, Y. Kato *ISIJ Int.* **2018**, 58, 620.

(35) G. Montante, K. C. Lee, A. Brucato, M. Yianneskis, *Computers and Chemical Engineering* **2001**, 25, 729.

(36) K. Shiobara, S. Hiraoka, Y. Kato, S. Iwata, T. Yamaguchi, *Kagaku kogaku ronbunsyu* **2007**, 33, 281.

(37) Y. Kato, H. Furukawa, K. Fujii, R. Nagumo, Y. Tada, S. T. Koh, Y. S. Lee, *Kagaku kogaku ronbunsyu* **2015**, 41, 215.

(38) T. W. Chapman, *AIChE J.* **1966**, 12, 395.

(39) M. V. Sardeshpande, A. R. Sagi, V. A. Juvekar, V. V. Rande, Ind. Eng. Chem. Res. **2009**, 48, 9713.

(40) S. Shimasaki, T. Wada, S.Taniguchi, *Tetsu-to-Hagane* **2003**, 89, 637.

(41) S. Nagata, K. Yamamoto, T. Yokoyama, S. Shiga, *Kagaku kogaku* **1957**, 21, 708.

(42) The Society of Chemical Engineering, *Handbook of Chemical Engineering*, Rev. 7th ed., Maruzen, Tokyo **2011**, P. 334.

Caption list

Figure 1 Schematic diagram of experimental apparatus and angle-changeable impeller blades.

Figure 2 Schematic diagram of PIV measurement system.

Figure 3 Schematic diagram of particles suspension patterns.

Figure 4 An example of suspension pattern of sedimentary particles (Resin-water, V_S/V_L=0.02, T=0.2 m, θ=40 deg, C=0.048 m).

Figure 5 An example of cross-sectional velocity vectors.

Figure 6 Effect of operating factors on transitions of particles suspension pattern.

Figure 7 Distribution of upward vertical mean velocity for different blade angle.

Figure 8 Comparison between measured and calculated *Fr* at the transition of I - II.

Figure 9 Comparison between measured and calculated *Fr* number (a) and N_{JS} by Tamburini et al. [30] at the transition of II – III and II' – III'.

Figure 10 Comparison between measured and calculated *Fr* at the transition of II - II' and III - III' (maximum rising height of particles).

Table 1 Physical properties of liquid phase at 298.15 K.

Table 2 Physical properties of solid particles.

Table 3 Experimental conditions of suspension pattern and PIV measurements.